

Local Chain Deformation and Overstrain in Reinforced Elastomers: An NMR Study

Roberto Pérez-Aparicio,[†] Martin Schiewek,[‡] Juan López Valentín,[§] Horst Schneider,[‡] Didier R. Long,[†] Marina Saphiannikova,^{||} Paul Sotta,[†] Kay Saalwächter,^{*,‡} and Maria Ott^{*,‡}

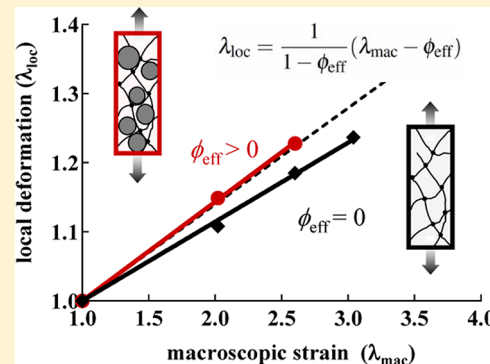
[†]Laboratoire Polymères et Matériaux Avancés, CNRS/Rhodia-Solvay, UMR 5268, 85 avenue des Frères Perret, F-69192 Saint Fons, France

[‡]Institut für Physik - NMR, Martin-Luther-Universität Halle-Wittenberg, Betty-Heimann-Str. 7, D-06120 Halle, Germany

[§]Institute of Polymer Science and Technology (ICTP-CSIC), C/Juan de la Cierva 3, 28006 Madrid, Spain

^{||}Leibniz-Institut für Polymerforschung Dresden e.V., Hohe Strasse 6, D-01069 Dresden, Germany

ABSTRACT: A molecular-level understanding of the strain response of elastomers is a key to connect microscopic dynamics to macroscopic properties. In this study we investigate the local strain response of vulcanized, natural rubber systems and the effect of nanometer-sized filler particles, which are known to lead to highly improved mechanical properties. A multiple-quantum NMR approach enables the separation of relatively low fractions of network defects and allows to quantitatively and selectively study the local deformation distribution in the strained networks matrix on the microscopic (molecular) scale. We find that the presence of nondeformable filler particles induces an enhanced local deformation of the matrix (commonly referred to as overstrain), a slightly increased local stress/stain heterogeneity, and a reduced anisotropy. Furthermore, a careful analysis of the small nonelastic defect fraction provides new evidence that previous NMR and scattering results of strained defect-rich elastomers cannot be interpreted without explicitly taking the nonelastic defect fraction into account.



I. INTRODUCTION

The understanding of the relationship between the mechanical behavior of elastomeric materials and the molecular, cross-linked, and topologically complex structure of their constituent polymer chains requires specific models predicting the loss in conformational entropy on deformation. Scattering methods, in particular neutron scattering with its potential to characterize the conformation of individually labeled probe chains, have proven useful to reveal strongly subaffine local deformations.^{1–5} These stand in strong contrast to predictions of the classical affine network model, and alternative approaches based upon, e.g., the phantom model, have been shown to provide a better match.^{1,6}

The analysis of scattering data is straightforward only in the case of networks made of labeled end-linked chains, while multiple statistically cross-linked (vulcanized) long chains have an overall complex deformation behavior, as affinity must ultimately be restored on large scales.⁷ Unfortunately, end-linked networks tend to have rather large fractions of nonelastic defects of 20% or more (such as dangling chain ends, short loops, sol), as shown in experiments⁸ and simulations.⁹ A separation of these defects is difficult for scattering data, but rather straightforward with appropriate NMR methods,¹⁰ and allows us to focus on the response of the elastically active network only.

Filled elastomers are an even bigger challenge for molecular-level studies of chain deformation by scattering methods and are the main focus of our work, using NMR as an alternative method. Filled rubbers exhibit substantially enhanced mechanical properties over their unfilled counterparts, which are due to a network formed by the filler particles, as well as the modified deformation behavior of the elastomer matrix and its constituent chains. The latter is commonly referred to as overstrain,¹¹ since the matrix surrounding undeformable filler particles must be deformed correspondingly more. This phenomenon is here studied for the first time in application-relevant rubber samples. For a homogeneous matrix filled with polydisperse hard spheres, the so-called hydrodynamic amplification factor A , defined as a ratio of the stress (or modulus) for a filled system to the stress for an unfilled system, reads^{12,13}

$$A \approx 1 + \frac{2.5\phi_{\text{eff}}}{1 - 2\phi_{\text{eff}}} \approx \frac{\lambda_{\text{loc}} - 1}{\lambda_{\text{mac}} - 1} \quad (1)$$

where ϕ_{eff} describes the effective filler volume fraction of the filled elastomer and $\lambda_{\text{mac}/\text{loc}}$ is the average macroscopic/local deformation of the network matrix. Equation 1 has commonly

Received: May 2, 2013

Revised: June 12, 2013

Published: June 28, 2013

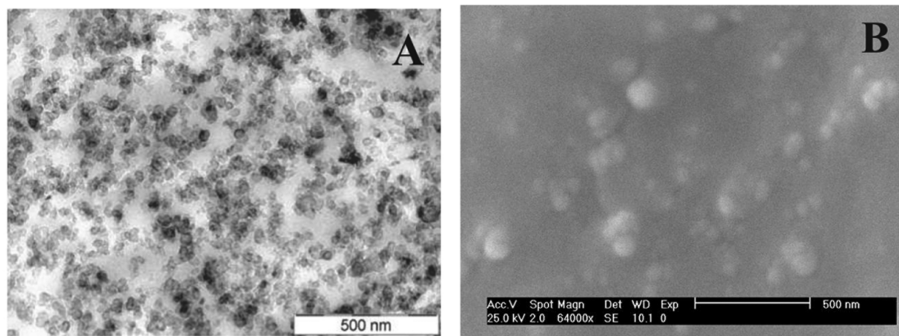


Figure 1. (A) TEM micrograph of a NR sample of series A (NR3A-S50-T) reinforced with 18.25 vol % of silica particles (Z1165 MP) treated with TESPT. The investigated samples are about 100 nm thick. (B) A representative SEM micrograph of a freeze-fractured NR sample of series B (40 phr of silica) demonstrates a poorer dispersion state of silica particles. The scale bars correspond to 500 nm.

been assumed to also hold for the local strain as shown by the last ratio in the equation, but very recent work has demonstrated this to be incorrect.¹⁴ With the correct amplification factor of the strain tensor $a = 1/(1 - \phi_{\text{eff}})$,^{15,16} the average local uniaxial deformation follows¹⁷

$$\lambda_{\text{loc}} = \frac{1}{1 - \phi_{\text{eff}}} (\lambda_{\text{mac}} - \phi_{\text{eff}}) \quad (2)$$

or equivalently

$$\frac{\lambda_{\text{loc}} - 1}{\lambda_{\text{mac}} - 1} = \frac{1}{1 - \phi_{\text{eff}}} \quad (3)$$

A successful molecular-level proof of the existence of overstrain could so far only be provided by neutron scattering of a model system made of mobile rubber chains suspended between phase-separated spherical high- T_g domains in a triblock copolymer, where the scattering of the spherical “fillers” can be matched away by suitable labeling.¹⁸ Similar studies trying to detect overstrain in more realistic filled elastomers have so far failed,¹³ which could well be due to the difficulties related to the necessity to match the large scattering of inorganic, inhomogeneously distributed fillers. A more indirect yet still rather local approach is the study of local deformation by monitoring the displacements of the nanometric filler particles by atomic force microscopy,¹⁹ which has evidenced overstrain following eq 1, yet molecular-level proof is still missing.

We use solid-state NMR spectroscopy to characterize local deformation distributions in stretched natural rubber systems through segmental orientation correlations. In particular, we analyze local inhomogeneities of local stretching in unfilled and filled samples and show clear evidence of overstrain in filled samples as compared to unfilled ones. Earlier, related work was almost exclusively restricted to the study of spectral splittings in deuteron (^2H) spectra of specifically labeled (and mostly unfilled) samples.^{20–28} Such splittings only arise in stretched samples, where they reflect the local orientation and the relative degree of stretching. It has been argued that the splittings mainly arise from the nonelastic defect fraction,²⁹ which is supported by the fact that similar splittings are also observed for low molar mass probe chains.²²

Besides providing a means to separate contributions from network defects, ^1H multiple-quantum (MQ) NMR provides a quantitative measurement of local segmental orientation correlations through the interproton residual dipole–dipole coupling constants D_{res} obtained from normalized double-

quantum (DQ) build-up curves. These are conveniently measured on low-field instruments using the mentioned MQ NMR technique following previously published procedures.^{10,30,31} The parameter D_{res} is directly related to a segmental orientation order parameter S_b :³⁰

$$D_{\text{res}} = D_{\text{eff}} S_b \quad (4)$$

where D_{eff} is the effective dipolar interaction constant representative of a statistical (Kuhn) segment; i.e., it comprises the preaveraging due to fast intrasegmental motions. In the unstretched state, S_b reflects the local density of active constraints (cross-links plus entanglements) or, equivalently, the inverse average number of segments N of the elastically active subchains in relation to their end-to-end distance R :³⁰

$$S_b = \frac{3}{5N} \left(\frac{R}{R_0} \right)^2 \sim F^2 \quad (5)$$

Here, $R_0^2 = Nb^2$ is the average equilibrium end-to-end distance with b as the segmental size. Equation 5 shows that S_b is proportional to the squared force, F^2 , acting on the ends of these subchains³² and hence serves as a microscopic (molecular) probe of strain and stress, which are proportional to each other on the local scale (in fact, they need to be in order to satisfy a constitutive relation). Importantly, with MQ NMR a possible distribution of $S_b \propto D_{\text{res}}$ can be analyzed in inhomogeneous samples.

The elastically effective local chain unit characterized by R and N can also be referred to as the “NMR submolecule” and defines the spatial resolution: it favorably reflects the shortest distance between combined cross-link and entanglement (tube) constraints to the anisotropic orientation fluctuations of its constituent segments. For example, natural rubber networks of an average molecular weight between cross-links of 1200 g/mol have an average end-to-end distance (R_0) of approximately 2.7 nm, assuming the molecular weight of a Kuhn segment to be identical to that of 1,4-polyisoprene.³³ Inhomogeneities are thus only detected if they arise on a length scale beyond a few (sub)network chains, for example, in spatial variations in cross-link density on a larger scale³⁴ or in swollen networks.³⁵

In this way, and in contrast to earlier NMR work that was merely focused on splittings in ^2H spectra that only arise in stretched samples ($\overline{R^2} \neq R_0^2$), and the direct comparison with the unstretched counterparts enables the determination of the local degree of stretching between closest active constraints, i.e., cross-links or entanglements:

Table 1. Comparison of the Apparent Molecular Weights between Cross-Links, $M_{c,\text{app}}$, and Filler Volume Fractions, ϕ , of All Samples Investigated in This Study^a

sample	$M_{c,\text{app}}$ (g/mol)	ϕ (vol %)	$\lambda = 1$			$\lambda = 2.6(*)/2.4(**)$		
			$\bar{D}_{\text{res}}/2\pi$ (Hz)	$\sigma_{\text{Dres}}/\bar{D}_{\text{res}}$	defects (vol %)	$\bar{D}_{\text{res}}/2\pi$ (Hz)	$\sigma_{\text{Dres}}/\bar{D}_{\text{res}}$	defects (vol %)
NR3A *	1102		280	0.06	6.0	401	0.40	7.2
NR2A-S50-T *	1428	18	216	0.12	4.5	420	0.76	7.3
NR2A-S50-O *	1575	18	196	0.20	5.2	338	0.80	6.6
NR1B **	2100		148	0.12	10.6	187	0.31	10.5
NR3B **	1200		260	0.10	4.1	311	0.40	3.8
NR2B-S20-T **	1750	7	175	0.35	22.2	238	0.42	29.8
NR2B-S50-T **	1600	18	193	0.74	32.3	249	0.62	32.2

^aThe average residual dipolar coupling constants, \bar{D}_{res} , and the relative widths of the corresponding distributions, $\sigma_{\text{Dres}}/\bar{D}_{\text{res}}$, as well as the defect volume fractions are given for the relaxed and one stretched state. The defect volume fractions of the stretched states are determined at the magic angle ($\Omega = 54.7^\circ$).

$$\frac{\bar{D}_{\text{res}}(\lambda_{\text{mac}})}{\bar{D}_{\text{res}}(\lambda_{\text{mac}} = 1)} = \frac{\overline{R^2}(\lambda_{\text{mac}})}{\overline{R^2}(\lambda_{\text{mac}} = 1)} \sim \lambda_{\text{loc,chain}}^2 \quad (6)$$

Complex, potentially inhomogeneous local deformation patterns can be revealed by the mentioned assessment of the D_{res} distribution. Note that $\lambda_{\text{loc,chain}}$ is expected to be lower than λ_{loc} and λ_{mac} in eqs 1–3 due to locally subaffine deformation. This must be considered in the assessment of a potential overstrain of the rubber matrix, for which the measured $\lambda_{\text{loc,chain}}$ of unfilled and filled samples are thus compared.

II. EXPERIMENTAL SECTION

Sample Preparation and Characterization. The polymer samples investigated in this work are natural *cis*-1,4 polyisoprene (natural rubber, NR). The samples from series A (NR3A and NR2A) consist of NR, specifically Standard Malaysian Rubber SMRSL. NR3A is identical to the sample 3a of ref 36. NR2A-S50-T and NR2A-S50-O were reinforced with 50 phr (phr denotes g per 100 g of rubber) of precipitated silica (Z1165 MP, Solvay), the volume fraction being 18.25%. Z1165 MP is a highly dispersible precipitated silica with average aggregate size of 50 nm and specific surface 160 m²/g (which corresponds to primary particle radius of the order of 10 nm). Silica is dispersed down to aggregate size as characterize by SAXS and TEM. A representative TEM picture is shown in Figure 1A. The silica surface was modified with a covering agent, *n*-octyltriethoxysilane (OCTEO, 4.1 phr), or a covalent coupling agent, bis(triethoxysilylpropyl)-tetrasulfane (TESPT, 4 phr), denoted as “-O” or “-T” in the sample names, respectively. Sulfur-vulcanized samples were obtained by a standard mixing/curing procedure where, first of all, rubber, vulcanization activators (4 phr of ZnO and 2 phr of stearic acid) and an antioxidant (1.9 phr of 6PPD) were blended in an internal mixer. Then, 1.5 phr of sulfur (vulcanizer), 2 phr of *N*-cyclohexyl-2-benzothiazolesulfenamide (CBS), and 0.2 phr of tetrabenzylthiuram disulfide (TBzTD) (accelerators) were added using an open roll mill at low temperature to avoid early cross-linking reaction. The curing times were determined by rheology curves measured by a Monsanto R100S oscillating disk rheometer. The uncured rubber films were vulcanized under pressure at 150 °C in a 2 mm thick plate mold.

The samples of series B (NR1B, NR2B, and NR3B) were made of NR from Standard Malaysian Rubber, SMRCV60. NR1B and NR3B are identical to the samples C-2 and C-5 of ref 37. NR2B-S20-T and NR2B-S50-T further contain 20 and 50 phr, respectively, of precipitated silica (Silica Ebrosil HA, Iquesil) modified with TESPT. Previous to the surface modification, silica particles were submitted to a sonication process using ethanol as a solvent. For this purpose, a VibraCell model VC 505 from Sonics & Materials Inc. (Newton, CT) was used, with an input energy of 18 kJ over a period of 7 min, while the sample dispersion was cooled down in an ice–water bath. Ultrasonic energy submitted to the system is able to partially break down the pristine aggregates and agglomerates. For surface

modification of silica particles, 10% w/w (with respect to the filler content) of TESPT and 8% w/w of diethylene glycol (with respect to the filler content) were incorporated to the reaction media, using ethanol as the solvent. After heating the reaction flask under reflux conditions for 1 h, the solvent was evaporated at room temperature overnight with a final drying step, at 70 °C for 2 h. The dispersion of modified silica is completely stable in ethanol media for days without any evidence about reaggregation.³⁸ A representative SEM micrograph of a freeze-fractured sample is shown in Figure 1B, demonstrating the presence of larger aggregates and thus poorer dispersion as compared to series A.

Table 1 gives a summary of all analyzed samples with the most important details about their composition. The filler volume fraction ϕ was determined as described in ref 38. The average molecular weight of the network chains between two cross-links, M_c , can be roughly estimated by the relation $M_c^{-1} = M_{c,\text{app}}^{-1} - M_e^{-1}$ using the experimentally derived apparent molecular weight $M_{c,\text{app}}$ and the nominal limiting value for entanglement dominated networks (M_e) known from literature. $M_{c,\text{app}}$ was determined by a relation derived from MQ NMR experiments (see below) which reads^{8,10}

$$M_{c,\text{app}} = \frac{617 \text{ Hz } f - 2}{\bar{D}_{\text{res}}/2\pi } \frac{f}{f} \text{ kg/mol} \quad (7)$$

The functionality f of the cross-links is herein set to 4, as unvulcanized NR chains have a high molecular weight between 10⁵ and 10⁶ g/mol. For all samples $M_{c,\text{app}}$ was found to be between 1100 and 2100 g/mol, which is well below $M_{e,\text{rheo}} \approx 3890$ g/mol.³⁹ Note that the factor $(f - 2)/f = 0.5$ in eq 7, related to the phantom model and first introduced in ref 8, was not considered in our earlier work. For instance, in refs 30 and 37 $\bar{D}_{\text{res,e}}/2\pi$ was estimated to about 70–90 Hz by an extrapolation based on results of equilibrium swelling experiments, corresponding to $M_{e,\text{NMR}}$ of around 7–9 kg/mol without the factor. This value compared favorably with a rheological $M_{e,\text{rheo}}$ of 6.2 kg/mol, which is however valid for polyisoprene with appreciable 3,4 microstructures. With the factor of 0.5, and comparing with the right $M_{e,\text{rheo}}$ for NR, good correspondence between $M_{e,\text{rheo}}$ and $M_{e,\text{NMR}} = 3.5\text{--}4.5$ kg/mol is retained. Table 1 also reports the defect fractions and the widths of the cross-link density distributions (distributions of $D_{\text{res}} \sim 1/M_{c,\text{app}}$), which are seen to be appreciable only for the filled samples of series B.

NMR Spectroscopy. The experiments were conducted on two different mq20 Bruker minispecs operating at 0.5 T with $\pi/2$ pulses of 2.6 and 1.95 μ s length and dead times of 11 and 15 μ s, respectively. Comparative experiments showed an overall good agreement of the operating systems and ensured the reproducibility of our findings. All experiments were conducted at temperatures between 70 and 98 °C ($T_g \sim -60$ °C measured by differential scanning calorimetry), allowing to remove not only initial but also strain-induced crystalline components (see below).

Orientation-Dependent Measurements of Strained Rubber Rings. The experimental determination of the strain response of the rubber systems was realized by die-cut sets of rubber rings which were

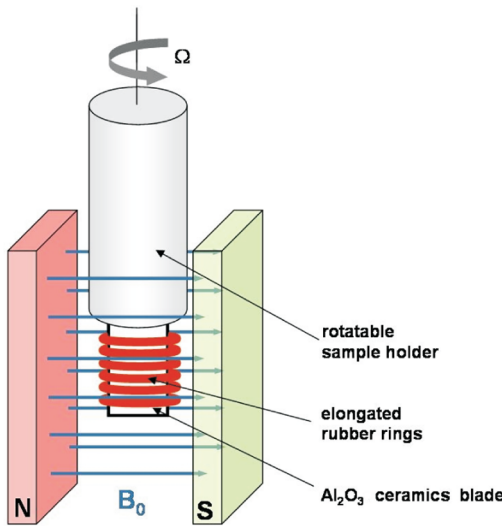


Figure 2. Experimental setup to measure elongated polymer networks. Strained rubber rings were stretched and slipped onto a thin Al_2O_3 ceramics blade. The sample holder was stepwise rotated to realize different orientations Ω with respect to the magnetic field B_0 . Orientation effects of the uniaxially stretched sample can be removed by construction of an artificial powder average by sampling different orientations of the stretched rubber rings, so as to be able to use a fitting procedure based upon a powder average.³¹

elongated to a length of approximately 10 mm and slipped onto a thin Al_2O_3 ceramics blade (Figure 2). Thus, a new sample was needed for each elongation value. The final elongation of the rings could be precisely varied by choosing the initial dimension of the rubber rings defined by the inner and outer diameters ($d_i = 1.5\text{--}3\text{ mm}$, $d_o = 3\text{--}4.5\text{ mm}$), with a ring width of 1–1.5 mm. The weighted average of the stretching parameter λ_{mac} was calculated by

$$\lambda_{\text{mac}} = \frac{l}{\pi} \frac{1/d_i - 1/d_o}{\ln(d_o/d_i)} \quad (8)$$

and is further used as a parameter to characterize the degree of deformation. The rotation of the sample was realized by a stepwise rotation of the ceramics blade using a computer-controlled servo motor (MSR 0020/L2-45-0, Mattke AG, Freiburg, Germany). The final accuracy was about 1°.

Powder Average Calculation To Remove Orientation Effects. NMR intensity data measured on a uniaxially strained sample are intrinsically subject to an orientation effect arising from the fixed angular relation between the strain direction and the B_0 field. Thus, some of the usual approaches for data analysis implying an isotropic powder distribution of anisotropic (here: dipolar) NMR interaction tensors may not be applicable. While a quasi-isotropic response can be obtained in principle by measurement of an isotropic powder sample of small uniaxially stretched network pieces, such an approach is of course technically not really feasible. However, orientation effects can also simply be removed (spatially averaged) by adding individual data sets taken at different evenly spaced orientations and using a weighting factor of $\sin \Omega$ to account for the orientation probability in a quasi-isotropic sample:

$$I_{\text{powder}} = \sum_i I(\Omega_i) \sin \Omega_i \quad (9)$$

Such an “artificial powder” successfully averages all orientation contributions of the dipolar interactions and hence allows to analyze the data according to established procedures of isotropic systems.³¹

Avoiding Effects of Strain-Induced Crystallization. Strain-induced crystallization (SIC) is an effect which occurs in NR and might have an impact on the measurements presented here.⁴⁰ Indeed, upon further stretching above the SIC onset, it has been shown that

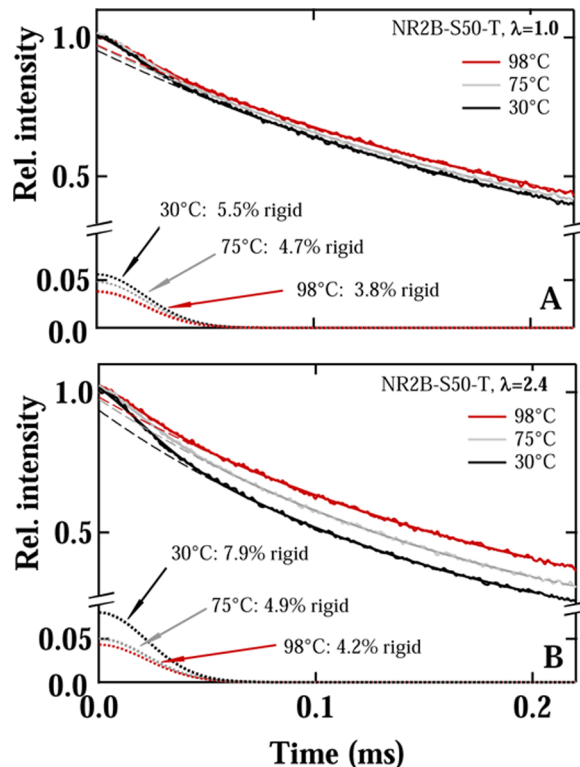


Figure 3. Normalized FID intensities after a dead-time free acquisition (magic sandwich echo pulse sequence) at different temperatures for the filled NR sample NR2B-S50-T without (A) and with applied strain (B). The two-component fitting functions (solid lines), consisting of a Gaussian (dotted) and a modified exponential (dashed), reveal solidlike and mobile contributions, respectively, as described in detail in ref 46.

the amorphous rubber orients less than it would in the absence of SIC.^{28,36,41} In pure NR matrices with cross-link densities comparable to the ones considered here, the SIC onset occurs at about $\lambda_{\text{mac}} = 3.5$ at room temperature and is shifted toward even higher λ_{mac} values as temperature increases. At $T = 70\text{ }^\circ\text{C}$ (the temperature of the measurements), the onset is at about $\lambda_{\text{mac}} = 5$ according to ref 42, which is well beyond the range investigated here. Kinetics measurements indicate that SIC is indeed a fast process,^{41,43,44} which means that equilibrated samples are measured on the time scale of our sample preparation and measurement.

In reinforced materials, at a given temperature, the SIC onset is shifted toward lower λ_{mac} values.^{28,45} However, at $70\text{ }^\circ\text{C}$ and above, the onset is shifted to values which are still beyond the range investigated here. Figure 3A,B shows exemplarily for one of the filled samples (NR2B-S50-T) that the signals of the stretched samples at temperatures above $70\text{ }^\circ\text{C}$ do not contain more rigid signal contributions as compared to the relaxed samples, which would come from crystallites. The fraction of rigid signal associated with noncrystalline material is due to impurities (proteins, lipids, etc.) that are also present in unfilled rubber and to immobile components related to the silica surface. We can thus conclude that SIC does not cause any appreciable problems for the investigated range of samples, elongations, and temperatures.

Determination of the Residual Dipolar Coupling Distributions of Polymer Networks by ^1H Multiple-Quantum NMR. The determination of the local distributions of the residual dipolar coupling constants, $p(D_{\text{res}})$, was realized by a multiple-quantum (MQ) NMR experiment as described elsewhere.^{10,31} Basically, the performed NMR experiment enables to acquire two sets of data. The DQ intensity $I_{\text{DQ}}(\tau_{\text{DQ}})$ mainly reflects DQ coherences which are dominated by the intrachain spin-pair coupling, and the reference intensity $I_{\text{ref}}(\tau_{\text{DQ}})$ includes all signal which has not evolved into DQ coherences after a

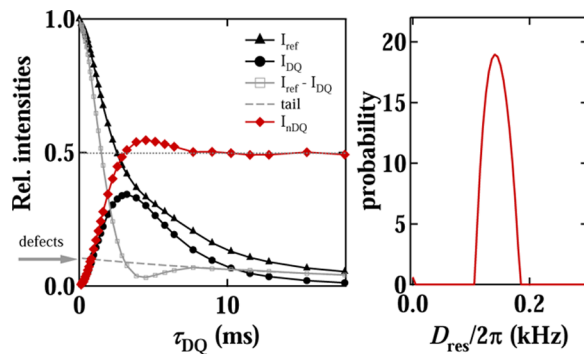


Figure 4. Left: an MQ experiment provides two intensity functions that relax for long evolution times τ_{DQ} : I_{DQ} (circles) and I_{ref} (triangles), as demonstrated for sample NR1B. The difference intensity $I_{\text{ref}} - I_{\text{DQ}}$ (squares) allows to reliably determine a tail function (dashed line) with an amplitude corresponding to the defect volume fraction of the sample (arrow). The overall intensity decay due to intermediate-time scale motions of the matrix can be removed by dividing I_{DQ} by the term $I_{\text{DQ}} + I_{\text{ref}} - \text{tail}$ for each τ_{DQ} (rhombi, red color). Right: the normalized DQ intensity I_{ndQ} enables to reveal distributions of the residual dipolar coupling by Tikhonov regularization.³¹

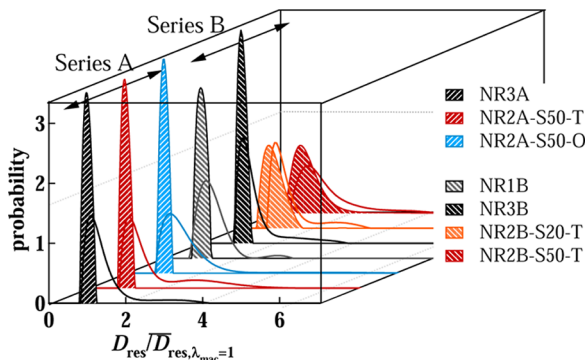


Figure 5. Distributions of D_{res} relative to the average value of the unstretched state $\bar{D}_{\text{res},\lambda_{\text{mac}}=1}$ in pure (black) and filled (colored) natural rubber without (filled areas) and with applied strain (lines). The macroscopic applied strains were $\lambda_{\text{mac}} = 2.60$ (series A) and $\lambda_{\text{mac}} = 2.42$ (series B).

certain evolution time τ_{DQ} (Figure 4). Consequently, the sum $I_{\text{sum}} = I_{\text{DQ}} + I_{\text{ref}}$ contains the full dipolar refocused intensities and can serve as a norm, which decays only due to molecular motions occurring on the time scale of the experiment. While these relaxation processes are present in both intensities, they can be removed by a point-by-point normalization. Contributions of nonelastic components (generally) do not contribute to I_{DQ} but lead to a slowly relaxing contribution to I_{ref} . In particular, the difference $I_{\text{diff}} = I_{\text{ref}} - I_{\text{DQ}}$ best reveals the nonelastic content of the sample. The long-time tail of $I_{\text{diff}}(\tau_{\text{DQ}})$ is a slowly decaying function which in our case can be well approximated by a single-exponential decay with an amplitude referring to the volume fraction of the defects (Figure 4).

A subtraction of the exponential tail from the sum intensity eliminates the defect contribution and a normalized DQ intensity build-up curve I_{ndQ} is obtained:

$$I_{\text{ndQ}}(\tau_{\text{DQ}}) = \frac{I_{\text{DQ}}(\tau_{\text{DQ}})}{I_{\text{DQ}}(\tau_{\text{DQ}}) + I_{\text{ref}}(\tau_{\text{DQ}}) - \text{tail}(\tau_{\text{DQ}})} \quad (10)$$

The build-up region of this function reflects the average D_{res} of the given sample, $I_{\text{ndQ}} \sim \langle \sin^2(kD_{\text{res}}\tau_{\text{DQ}}) \rangle \propto \langle D_{\text{res}}^2 \rangle \tau_{\text{DQ}}^2$, and information on a potential distribution of D_{res} values is reflected in its exact shape, specifically in increasingly early deviations from a quadratic initial rise. The determination of the distribution function, based upon a known

build-up function for the single- D_{res} case,³¹ is an ill-posed problem but can be realized by regularization methods. We applied a method that was specifically designed for polymer networks and is based on an experimentally derived build-up kernel function.³¹ This approach has the advantage that not only the initial part of the normalized build-up curve but all points up to the plateau value of 0.5 are included. It enables to access a broad range of dipolar interactions and to reveal possible inhomogeneities. The determinations of the average dipolar interactions and the distribution widths were accomplished by deriving the weighted average and the second moment of the resulting distributions. The integration interval over the distribution was set such that small contributions at very high dipolar interactions, which are not related to the network response but arise from intensity uncertainties at small τ_{DQ} were excluded from analysis. Note that the quantitative analysis of $I_{\text{ndQ}}(\tau_{\text{DQ}})$ is based upon an isotropically powder-averaged signal and is hence not directly applicable to the response of a strained and thus anisotropic sample measured for a single orientation, as addressed above.

III. RESULTS AND DISCUSSION

In the following, we study the changes in D_{res} and its distribution, thus the corresponding strain inhomogeneities arising in uniaxially strained samples to reveal the potential impact of embedded filler particles onto the local network deformation. For this purpose we investigated two series of vulcanized natural rubber samples, based upon high-molecular-weight precursor polymers. The process of vulcanization ensures that the polymer chains are well cross-linked and the defect fraction is comparably low. Some of the samples contained further silica filler particles with details given in Table 1. The silica dispersion of all filled samples is typical for application-relevant (tire) preparations, characterized by a coexistence of isolated, aggregated, and aggregated silica structures (see Figure 1).

D_{res} Distributions of Unstrained Networks. Although the expected chain length distribution of statistically cross-linked samples should lead to a broad distribution of D_{res} (or equivalently S_b), we found in agreement with previous results²⁹ the D_{res} distributions for the unstrained samples to be very narrow, thus characterizing rather homogeneously cross-linked rubbers (Figure 5). Even rubber samples containing nanometer-sized filler particles revealed homogeneous and unimodal distributions, indicating that effects arising from immobilized polymer chains or cross-link density inhomogeneities in proximity of filler particles are weak if not negligible. Such high homogeneities of the samples are needed to be able to uniquely and unambiguously resolve the actual strain-induced network response. It should be noted that the high homogeneity of our sample series A cannot be taken for granted as e.g. poly(ethyl acrylate)-based networks with tunable model filler dispersion exhibit much broader distributions for filled and pure systems indicative of complex and inhomogeneous cross-linked structures^{47,48} and thus cannot be used for the present purpose.

Local Chain Stretching and Orientation in Strained Networks. Stretched states have been realized by elongation of rubber rings of different inner and outer diameters where the maximum value of λ_{mac} is limited by the mechanical stability of each sample. In such uniaxially stretched (thus anisotropic) samples, the DQ build-up curves become orientation-dependent. This dependence is a very valuable source of information, but since suitable theories for its analysis are not yet available and currently under development in our laboratories, a detailed account is deferred to a later publication.

We thus mainly focus on the average stretching state, which was characterized by orientation-dependent sampling with respect to the magnetic field (see Figure 2). The resulting distributions of local deformations shown in Figure 5 clearly reveal a strain-induced overall increase of the average D_{res} ; in particular, they show a population of highly strained chains as reflected in the high-coupling tail or sometimes a second peak. Note that the appearance of a peak rather than a tail may well be a numerical artifact of the regularization procedure. Importantly, the overall shapes of the distributions, in particular their mean and width (standard deviations), were robust within reasonable choice of the error-related parameter of the fitting routine.³¹ The widths of the distributions reflect the heterogeneity of the local chain stretching under macroscopic elongation. For a quantitative understanding, we are currently working on implementing appropriate local-deformation models that have been used previously to explain neutron scattering results on strained networks. The background is, simply put, that chains with end-to-end vectors initially oriented parallel or perpendicular to the stretching direction are expected to be deformed differently, i.e., being either strongly stretched or even slightly compressed, respectively. This will enable a critical test of different network models but is beyond the present scope, where we focus on the specific effects in filled samples.

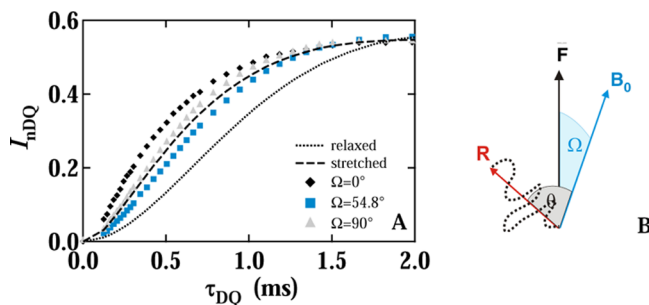


Figure 6. (A) Normalized DQ intensity build-up $I_{\text{ndQ}}(\tau_{\text{DQ}})$ for the sample NR3A at $\lambda_{\text{mac}} = 3$ and different orientations with respect to the magnetic field (symbols) along with the constructed powder average (dashed line). The dotted line represents the response without applied strain. (B) A polymer chain with end-to-end distance R with respect to the magnetic field and the applied force.

To highlight the potential of the new approach, we qualitatively demonstrate the anisotropic feature of the highly oriented network chains in stretched samples. This is realized by plotting the normalized DQ intensities for individual orientations (Figure 6A). The normalized DQ intensity, I_{ndQ} , is expressed as a time and ensemble average of the individual polymer chain signals, which may be written as

$$I_{\text{ndQ}}(\tau_{\text{DQ}}) = \langle \sin^2(\omega_{\text{res}}(R^2, \theta)\tau_{\text{DQ}}) \rangle \quad (11)$$

The individual residual interaction frequency $\omega_{\text{res}}(R^2, \theta) \sim D_{\text{res}}(R^2)P_2(\cos \theta)$ depends on the stretching and second Legendre polynomial of the orientation θ of the chain (see Figure 6B). In a system with uniaxial symmetry, the ensemble average then shows a typical “magic angle effect”, in which the average residual interaction has a clear minimum at the magic angle of 54.7° (corresponding to the minimum of $|P_2(\cos \theta)|$). This effect is observed in Figure 6A and even more clearly in the angle-dependent integral nDQ signal intensities plotted in Figure 7A.

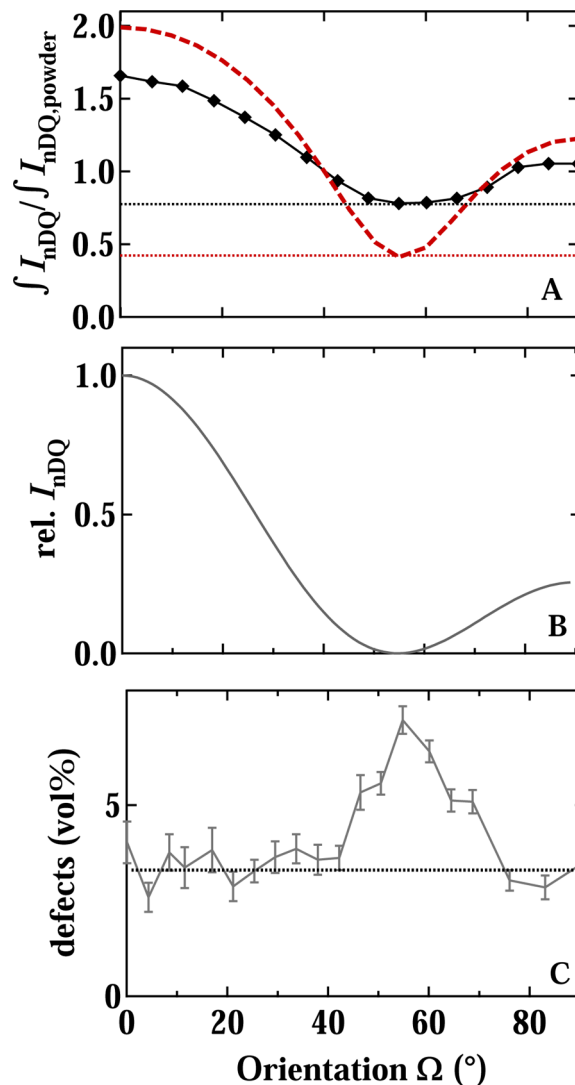


Figure 7. Network chain vs defect response: (A) Angular dependence of I_{ndQ} for NR3A at $\lambda_{\text{mac}} = 3.0$ (integral of the signal up to a fixed relative τ_{DQ} time), renormalized by the corresponding powder-averaged value (symbols) in comparison with the Gaussian model (red, dashed line). (B) Theoretical angle dependence of I_{ndQ} for defect chains. (C) Angle dependence of the measured apparent fraction of defect chains.

However, the experimental data show a much weaker angle dependence than predicted theoretically by the junction-affine model, which is based upon an affinely deformed, quasi-static Gaussian distribution of end-to-end distances (see Figure 7A). Nevertheless, we have chosen to use this model as it allows to discuss in a simple way whether local deformations are affine or not under macroscopic extension. The quasi-static Gaussian-chain model is the only elementary model that has been used so far to attempt a theoretical description of previous NMR data,^{20,21,25,49–51} sometimes including ad-hoc assumptions on additional orientation correlations.^{20,25,50,51} It describes the network to be made of fluctuating chains which have a quasi-static Gaussian distribution of end-to-end distances⁵² and are attached to fixed, nonfluctuating end points whose positions are deformed affinely under macroscopic strain.⁵³ The weaker angular dependence demonstrated in Figure 7A indicates that macroscopic deformations lead to force-equilibrated rearrangements on the molecular level and hence to a local deformation

which is less than affine. This will be addressed in detail in future work.

Influence of Network Defects. While long defect (nonelastic) chains may be topologically constrained within the cross-linked rubber matrix (trapped entanglements, loops) and thus behave like proper cross-linked network chains, shorter defects (dangling chains) are able to diffuse more freely and only reflect the average anisotropy of the accessible volume. Free ends of defect chains move in the fast limit, which averages intrasegmental couplings down to a value representing the anisotropy of intersegmental excluded-volume interactions with the neighboring chains. Hence, dangling chains act as a local probe and their residual coupling reflects the mean anisotropy and orientation of their accessible volume. This has been exploited widely in terms of residual quadrupolar splittings in ^2H spectra of deuterated small molecules or unlinked probe chains in stretched network samples.^{20,22,27,54–58} Consequently, for an unstrained (isotropic) network the anisotropic NMR interactions within defect chains average to zero, as also illustrated by ^2H spectra, which exhibit a sharp central peak.^{22,54,55,58,59}

In consequence, the residual coupling, and with it I_{DQ} according to eq 11, arising for the defect contributions exhibits an orientation dependence which follows exactly the second Legendre polynomial of the angle between the strain direction and B_0 . This is because the D_{res} induced in defect chains, which arises from a diffusional average, has a perfect correlation with the *macroscopic* deformation. This stands in contrast to network chains, which have fixed orientations that vary within the sample (see Figure 6B). As indicated in Figure 7B, the D_{res} and thus the associated DQ intensity of the defect contribution are predicted to now cancel completely at the magic angle.

Consequently, the *apparent* defect fraction extracted from an MQ experiment on a strained sample (which corresponds to components with zero coupling) should be separable from the matrix response at the magic angle. Indeed, as is exemplarily shown in Figure 7C, we find maximal defect fractions at around the magic angle (e.g., $7.2 \pm 1\%$ for NR3A and $3.8 \pm 0.5\%$ for NR3B), which are further within error consistent with the defect fractions of the unstretched rubber (e.g., $6.0 \pm 0.5\%$ for NR3A and $4.1 \pm 0.5\%$ for NR3B); see also Table 1. The remaining low amount of $\sim 3\%$ at other orientations may be related to the nonuniaxially strained parts of the samples at edges or perhaps to other defects such as low molecular weight compounds. We can conclude that the average residual dipolar coupling measured in stretched elastomers generally does not only reflect the local deformation of the network only but also includes the orientation effect of the defect chains described above. This is of importance for defect-rich samples (and hence concerns two of the more inhomogeneous filled samples of series B) but can safely be neglected for samples with defect fractions of less than ≤ 10 vol %, such as all other samples investigated herein.

Changes of D_{res} and Its Distribution in Strained Networks. The relative increase of the average (distribution-averaged) residual dipolar interaction, $\bar{D}_{\text{res}}(\lambda_{\text{mac}})/\bar{D}_{\text{res}}(\lambda_{\text{mac}} = 1)$, of elongated samples is plotted in Figure 8A. It is found to be far less than predicted by the affine Gaussian model. Most importantly, this subaffine behavior must arise from the chemically cross-linked network itself, since possible influences of defect chains and large entanglement effects are of minor relevance in our case (the molecular weights of the network chains in most samples are well below the limiting value for

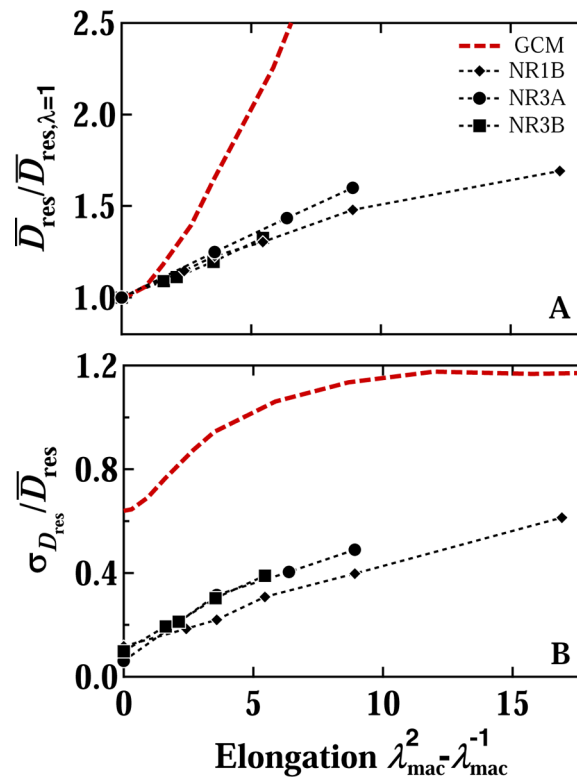


Figure 8. (A) Relative average residual dipolar coupling \bar{D}_{res} and (B) the corresponding relative distribution widths $\sigma_{D_{\text{res}}}/\bar{D}_{\text{res}}$ as a function of the strain function for the different unfilled systems (symbols) in comparison with the prediction of the quasi-static Gaussian chain model (red dashed line).

entanglement-dominated networks). The initial slope of the “relative deformation” was further independent of the cross-link density and details in the sample preparation, in contrast to results reported in ref 24.

Further evidence of significant deviations from the affine quasi-static Gaussian chain model is given by the rather low local anisotropy (Figure 7A) and the narrow local deformation distributions, $\sigma_{D_{\text{res}}}/\bar{D}_{\text{res}}$ plotted in Figure 8B. Here, $\sigma_{D_{\text{res}}}$ is the numerically calculated standard deviation of the distribution obtained from the regularization procedure. We note on the side that a detailed reanalysis of the spectral components of various polymer network systems from the literature, e.g. refs 21, 25, 49, 60, and 61, is in agreement with our findings, as will be reported in a separate publication. In short, we were able to model the published ^2H NMR spectra as a superposition of a narrow component with fast isotropic motions (from network defects, sol, etc.) and a broad Gaussian-like contribution of the network. The spectral width of the latter, related to the residual quadrupolar coupling, follows the same trend as our data in Figure 8A.

The failure of the quasi-static Gaussian model to describe strained networks is in fact not surprising in light of the fact that even in the bulk unstrained state the distribution of local order parameters is experimentally found to be much narrower than predicted. One reason for this lies at hand: as opposed to scattering results, the NMR observable represents a *time average*, while the model implicitly assumes a frozen-in end-to-end distribution.^{49,50} According to phantom-type (and possibly also tube-based) models, which according to our previous work fit NMR and swelling data much better,⁸ the cross-link

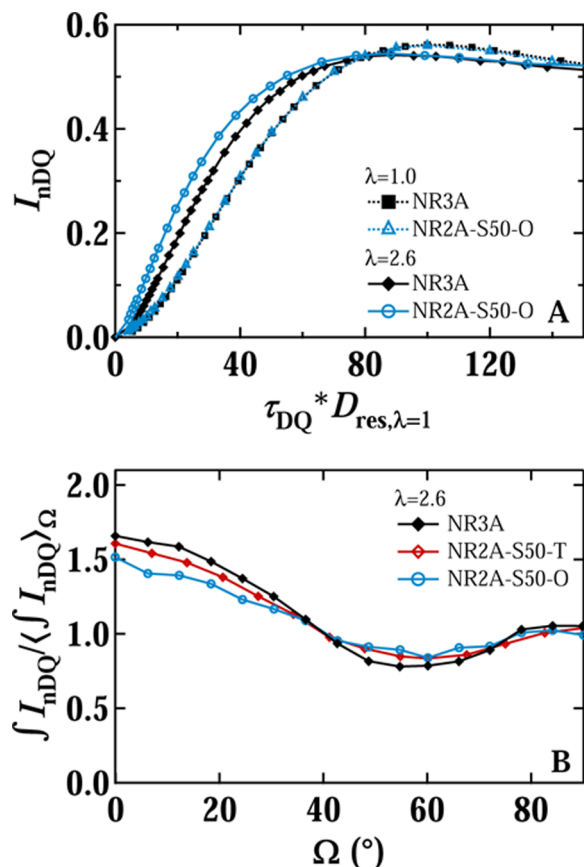


Figure 9. (A) Normalized DQ intensities I_{ndQ} (“artificial” powder averages) for pure (closed symbols) and filled (open symbols) NR samples of series A with and without applied strain, plotted on a mastered time axis. (B) Corresponding angular dependences of I_{ndQ} (integral of the signal up to a fixed relative τ_{DQ} time, renormalized by the powder-averaged value). The data directly reveal a locally enhanced strain (A) and a reduced anisotropy (B) for the filled samples.

fluctuations lead to a partial mapping out of the end-to-end distribution during the time average, whereby an at least partially ensemble-averaged order parameter and a correspondingly narrow distribution arise. Moreover, these fluctuations possibly allow force equilibration between different chains attached to a given cross-link³² and thus a homogenization of the observed D_{res} values. As noted, these aspects are deferred to our future work, and we turn to the quantitative measurement of overstrain, which is independent of the details of the chain-deformation model.

Local Deformation of the Network Matrix in the Presence of Nanoscopic Filler Particles. Figure 9A compares the normalized DQ build-up curves for a filled and unfilled sample of series A on a mastered time axis. For the unstretched case, since the nDQ build-up curves depend only on the product of the residual dipolar interaction and the evolution time ($I_{ndQ} \sim \langle \sin^2(kD_{res}\tau_{DQ}) \rangle$), we can perfectly superimpose the curve shapes of the filled and unfilled samples by rescaling the time axis according to their respective D_{res} values. This indicates the same (or similar) underlying distribution of residual dipolar interactions. In other words, the unfilled and filled samples of this series feature a similarly homogeneous rubber matrix. Turning to the stretched samples, the overstrain becomes immediately apparent in this scaled

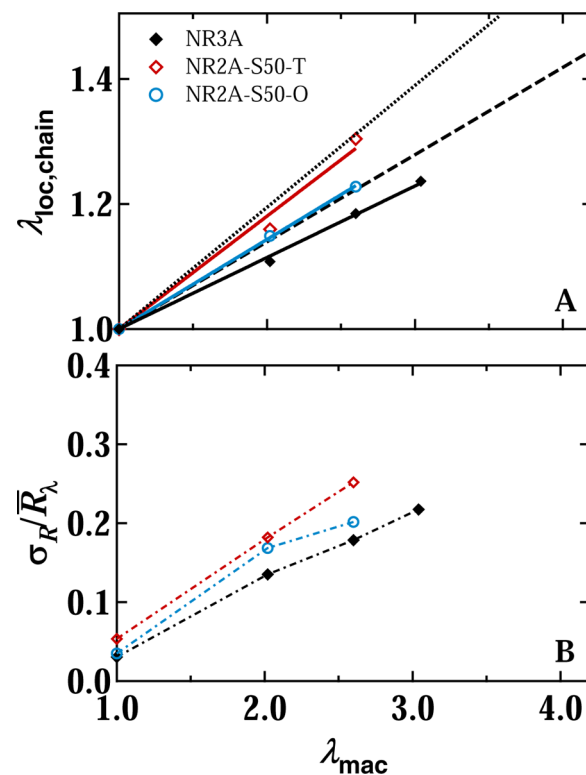


Figure 10. (A) Relative local deformations $\lambda_{loc,chain} = \bar{R}/\bar{R}_{\lambda_{mac}=1}$ and (B) the corresponding distribution widths $\sigma_R/\bar{R}_{\lambda}$ upon macroscopic deformation λ_{mac} for unfilled (closed symbols) and filled (open symbols) systems of series A. The solid lines in (A) are linear fits quantifying the nonaffinity in the unfilled sample and the overstrain in the filled samples (see text). The dotted and dashed lines are predictions based upon eqs 1 and 3, respectively, assuming $\phi_{eff} = \phi$.

representation, as the build-up curve of the strained filled sample is different from and rises more quickly than the curve of the unfilled counterpart (both samples differ somewhat in D_{res} , but the scaled time axis accounts for this difference).

Moreover, the addition of filler particles does not increase but even slightly decreases the orientation dependence, and thus the local anisotropy of the network structure, as demonstrated in Figure 9B. This effect may originate from restrictions of local chain rearrangements by filler particles or from nonaffine displacements of filler particles, if e.g. the filler particles are topologically linked. In both cases the presence of filler particles would preserve the local isotropy of the attached network chains and hence reduce the anisotropic feature.

The local strain and overstrain in the filled samples as well as their inhomogeneity are addressed in Figures 10A and 10B, respectively. The overstrain describes the enhanced average local deformation of polymer chains in filled compared to unfilled rubber systems at the same macroscopic elongation. It can be experimentally estimated either by comparing the macroscopic deformation of unfilled and filled systems which induce the same average microscopic deformation⁴⁵ or by directly comparing the average microscopic deformations of both systems as described by eq 1 or 3.

We follow the latter strategy and first address the actual average local deformation $\lambda_{loc,chain} = \bar{R}/\bar{R}_{\lambda_{mac}=1}$. This corresponds to the weighted (relative) average of the end-to-end distance distribution, $p(R)$, which for MQ NMR experiments ($R^2 \sim$

D_{res}) can be directly derived from the corresponding D_{res} distribution, $p(D_{\text{res}})$, using

$$\bar{R} = \int_0^\infty R p(R) dR \sim \int_0^\infty \sqrt{D_{\text{res}}} p(D_{\text{res}}) dD_{\text{res}} \quad (12)$$

We note that the root-mean-square average $(\bar{R}^2)^{1/2} \sim (\bar{D}_{\text{res}})^{1/2} = (\int D_{\text{res}} p(D_{\text{res}}) dD_{\text{res}})^{1/2}$ corresponds to the second moment of the R distribution and thus gives larger values for broad distributions. As second moments are generally more sensitive to uncertainties in the amplitude of components with high parameter values, we use eq 12, which provides a realistic lower limit.

Now, before turning to the filled samples, we need to take into account that the chain-level $\lambda_{\text{loc,chain}}$ is much lower than λ_{mac} for unfilled rubber samples due to the locally nonaffine deformation. The data for unfilled samples shown in Figures 8A and 10A suggest a near-linear subaffine behavior in the range $\lambda_{\text{mac}} \leq 3$, and a fit to the data for NR3A yields $(\lambda_{\text{loc,chain}} - 1) = 0.11 \times (\lambda_{\text{mac}} - 1)$. Assuming this subaffinity to arise on a length scale shorter than the filler particle size, we can thus replace $(\lambda_{\text{loc}} - 1)$ in eqs 1 and 3 by $(\lambda_{\text{loc,chain}} - 1)/0.11$.

A simple comparison of the slopes of the linear fits to the filled and unfilled sample data in Figure 10A immediately reveals a nearly constant strain amplification of 1.25 and 1.8 for NR2A-S50-O and NR2A-S50-T, respectively. This is well above the uncertainties of our measurement but below the theoretical prediction of eq 1 assuming $\phi_{\text{eff}} = \phi = 0.18$ (dotted line in Figure 10A). This is not surprising, considering its recently identified nonapplicability.¹⁴ We remind, however, that eq 1 has been used as a gauge in previous work.^{18,19} The correct hydrodynamic prediction, eq 3 with $\phi_{\text{eff}} = \phi = 0.18$, shown as dashed line in Figure 10A, underpredicts the result for NR2A-S50-O only slightly and can be made to match the linear fit results for both filled samples by simply adjusting the value of ϕ_{eff} to 0.20 and 0.37 for NR2A-S50-O and NR2A-S50-T, respectively.

We remind that the NMR method provides a measure of local deformation, which is in principle proportional to the elongation R/R_0 of the elastically active strand (see eq 5). The observed deviation may thus also arise from the average over an inhomogeneous and complex distribution, which is ultimately one of the reasons why the distinction between eqs 1 and 3 has to be made.¹⁴ The width of the distribution of local strain as a function of strain is plotted in Figure 10B and shows indications of increased inhomogeneity in the latter. Generally, our results on the distribution function of local strain (and thus local stress) (see also Figure 5) will certainly be of use to address this problem more fundamentally. The local deformation distributions of the polymer networks indeed indicate that the macroscopically applied forces are transmitted by a small fraction of highly strained network chains (those initially oriented along the stretching direction), while large parts of the networks are less strained and may even reorganize on the mesoscopic scale.⁶² We stress that in sample series A, in which fillers are well dispersed, the inhomogeneity of the local strain (or stress) in the filled samples increases near-linearly and similarly to that of the pure system (Figure 10B). The differences between the samples surface-modified with OCTEO and TESPT in both the average local strain and its distribution at larger external strain may well arise from the differences in polymer–silica interaction or differences in the dispersion state.

Analogous results for $\lambda_{\text{loc,chain}}$ and σ_R/\bar{R}_λ for the samples of series B, as compiled in Figures 11A and 11B, respectively,

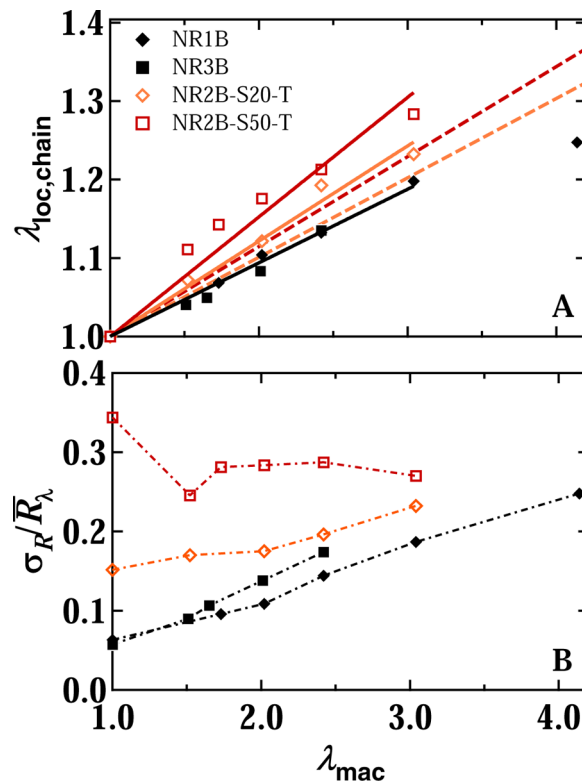


Figure 11. (A) Relative local deformations $\lambda_{\text{loc,chain}} = \bar{R}/\bar{R}_{\lambda_{\text{mac}}=1}$ and (B) the corresponding distribution widths σ_R/\bar{R}_λ upon macroscopic deformation λ_{mac} for unfilled (closed symbols) and the more inhomogeneous filled samples (open symbols) of series B. The solid lines are linear fits quantifying the overstrain and revealing an increased $\phi_{\text{eff}} > \phi$ (see text), and the dashed lines are based upon predictions of eq 3 assuming $\phi_{\text{eff}} = \phi$.

support the latter assumption. While the unfilled samples of this series (filled symbols) are comparable to those of series A, $(\lambda_{\text{loc,chain}} - 1) = 0.09 \times (\lambda_{\text{mac}} - 1)$, the filled counterparts exhibit a somewhat higher apparent cross-linking heterogeneity in the unstretched state (see Table 1) and a more pronounced filler aggregation (see Figure 1B). The filled samples exhibit a significantly higher initial strain amplification, and linear fits for the larger range $\lambda_{\text{mac}} \leq 3$ yield 1.33 and 1.67 for NR2B-S20-T and NR2B-S50-T, respectively; see Figure 11A). Expectedly, almost no strain-induced effect on the distribution widths can be identified (Figure 11B). The overstrain depends, as expected, on the filler loading. These observations, in particular the decisive nonlinearity of the $\lambda_{\text{loc,chain}}$ data for NR2B-S50-T, evidence a complex and nonlinear response in terms of local deformation. The overall higher overstrain values might be induced by a higher ϕ_{eff} due to volume occlusions in between filler aggregates. Equation 3 yields $\phi_{\text{eff}} = 0.23$ and 0.38, to be compared with $\phi = 0.07$ and 0.18 for NR2B-S20-T and NR2B-S50-T, respectively. For a detailed understanding, we are planning to correlate these observations with the nonlinear mechanical properties (Payne effect) following our recent work,⁶³ and more quantitative studies of the filler dispersion using scattering techniques.⁶⁸ The latter were beyond the scope of the present effort.

IV. CONCLUSION

In summary, we were able to reveal for the first time on a local (molecular) scale a significant overstrain of active elastic

subchains in filled, application-relevant elastomers. Our results further indicate a qualitative effect of filler particle distributions on the local response. Our lower-limit estimate of the matrix overstrain is in quantitative agreement with a recently identified appropriate hydrodynamic prediction.^{14,17} The revealed complexity of the responses in terms of inhomogeneous distributions of local strain/stress as well as the reduced overall anisotropy observed in filler samples demonstrate the capability of the introduced NMR method to reveal local effects. Our results also stress the need of initially homogeneous and possibly tunable particle distributions in experiments aimed at a complete understanding of network elasticity and the role of overstrain as compared to filler networking.

Our molecular-level data reporting on local stress/strain for both unfilled and filled natural rubber samples could not be described by the affine quasi-static Gaussian-chain model that was previously used to describe NMR data. The pronounced homogeneity in unstretched samples, the clearly subaffine local stress/strain response, and the reduced anisotropy indicate that the local network structure can adapt to a significant degree; thus, the junctions are clearly not affinely deformed, in agreement with previous scattering studies. Theoretical approaches to model the experimental data of the unfilled samples based upon phantom or tube model ideas are currently under development.

From the changes in the apparent amount of the detected, isotropically mobile defect chains, we inferred further evidence that the most often discussed spectral splittings observed in ²H NMR spectra of various (mostly defect-rich model-type) elastomers originate from dangling chain ends and cyclic structures that do not support stress, rather than from the network itself. The anisotropic excluded-volume effect of the surrounding matrix, possibly combined with an increased apparent entanglement density,⁶⁴ provides an additional anisotropic constraint that leads to a residual orientation of the defect chains. This is of relevance not only for the NMR response of the network chains but also for network elasticity in general.^{51,65–67}

AUTHOR INFORMATION

Corresponding Author

*E-mail: kay.saalwaechter@physik.uni-halle.de (K.S.); maria.ott@physik.uni-halle.de (M.O.).

Notes

The authors declare no competing financial interest.

ACKNOWLEDGMENTS

The authors thank Arnaud Vieyres and Olivier Sanséau (LPMA CNRS/Rhodia-Solvay) for fruitful discussions. Funding was provided by the DFG-ANR German-French joint project "DINaFil", SA982/6-1. J.L.V. thanks Secretaría de Estado de Investigación, Desarrollo e Innovación (Spain), for his Ramon y Cajal contract.

REFERENCES

- (1) Erman, B. Chain dimensions in deformed networks: theory and comparison with experiment. *Macromolecules* **1987**, *20*, 1917–1924.
- (2) Beltzung, M.; Picot, C.; Herz, J. Investigation of the chain conformation in uniaxially stretched poly(dimethylsiloxane) networks by small-angle neutron scattering. *Macromolecules* **1984**, *17*, 663–669.
- (3) Hinkley, J. A.; Han, C. C.; Mozer, B.; Yu, H. Chain deformations in rubber. *Macromolecules* **1978**, *11*, 836–838.

(4) Clough, S. B.; Maconnachie, A.; Allen, G. Small-angle neutron scattering from stretched polystyrene networks. *Macromolecules* **1980**, *13*, 774–775.

(5) Bastide, J.; Duplessix, R.; Picot, C.; Candau, S. Small angle neutron scattering and light spectroscopy investigation of polystyrene gels under osmotic deswelling. *Macromolecules* **1984**, *17*, 83–93.

(6) Ullman, R. Small-angle neutron scattering from elastomeric networks. Junction fluctuations and network unfolding. *Macromolecules* **1982**, *15*, 582–588.

(7) Ullman, R. Small-angle neutron scattering from elastomeric networks. Application to labeled chains containing several crosslinks. *Macromolecules* **1982**, *15*, 1395–1402.

(8) Chassé, W.; Lang, M.; Sommer, J.-U.; Saalwächter, K. Cross-link density estimation of PDMS networks with precise consideration of networks defects. *Macromolecules* **2012**, *45*, 899–912.

(9) Gilra, N.; Cohen, C.; Panagiotopoulos, A. Z. A Monte Carlo study of the structural properties of end-linked polymer networks. *J. Chem. Phys.* **2000**, *112*, 6910–6916.

(10) Saalwächter, K. Proton multiple-quantum NMR for the study of chain dynamics and structural constraints in polymeric soft materials. *Prog. Nucl. Magn. Reson. Spectrosc.* **2007**, *51*, 1–35.

(11) Mullins, L.; Tobin, N. R. Stress softening in rubber vulcanizates. Part I. Use of a strain amplification factor to describe elastic behavior of filler-reinforced vulcanized rubber. *Rubber Chem. Technol.* **1966**, *39*, 799–813.

(12) Christensen, R. M. *Mechanics of Composite Materials*; Wiley: New York, 1979.

(13) Botti, A.; Pyckhout-Hintzen, W.; Richter, D.; Urban, V.; Straube, E. A microscopic look at the reinforcement of silica-filled rubbers. *J. Chem. Phys.* **2006**, *124*, 174908–5.

(14) Domurath, J.; Saphiannikova, M.; Ausias, G.; Heinrich, G. Modelling of stress and strain amplification effects in filled polymer melts. *J. Non-Newtonian Fluid Mech.* **2012**, *171–172*, 8–16.

(15) Ahamadi, M.; Harlen, O. G. Numerical study of the rheology of rigid fillers suspended in long-chain branched polymer under planar extensional flow. *J. Non-Newtonian Fluid Mech.* **2010**, *165*, 281–291.

(16) Castañeda, P. P.; Tiberio, E. A second-order homogenization method in finite elasticity and applications to black-filled elastomers. *J. Mech. Phys. Solids* **2000**, *48*, 1389–1411.

(17) Govindjee, S.; Simo, J. A micro-mechanically based continuum damage model for carbon black-filled rubbers incorporating Mullins' effect. *J. Mech. Phys. Solids* **1991**, *39*, 87–112.

(18) Westermann, S.; Kreitschmann, M.; Pyckhout-Hintzen, W.; Richter, D.; Straube, E.; Farago, B.; Goerigk, G. Matrix chain deformation in reinforced networks: a SANS approach. *Macromolecules* **1999**, *32*, 5793–5802.

(19) Lapra, A.; Clément, F.; Bokobza, L.; Monnerie, L. Straining effects in silica-filled elastomers investigated by atomic force microscopy: from macroscopic stretching to nanoscale strainfield. *Rubber Chem. Technol.* **2003**, *76*, 60–81.

(20) Deloche, B.; Samulski, E. T. Short-range nematic-like orientational order in strained elastomers: a deuterium magnetic resonance study. *Macromolecules* **1981**, *14*, 575–581.

(21) Gronski, W.; Stadler, R.; Marly Maldaner, J. Evidence of nonaffine and inhomogeneous deformation of network chains in strained rubber-elastic networks by deuterium magnetic resonance. *Macromolecules* **1984**, *17*, 741–748.

(22) Sotta, P.; Deloche, B.; Herz, J.; Lapp, A.; Durand, D.; Rabadeux, J. C. Evidence for short-range orientational couplings between chain segments in strained rubbers: a deuterium magnetic resonance investigation. *Macromolecules* **1987**, *20*, 2769–2774.

(23) Dubault, A.; Deloche, B.; Herz, J. Effects of trapped entanglements on the chain ordering in strained rubbers: a deuterium magnetic resonance investigation. *Macromolecules* **1987**, *20*, 2096–2099.

(24) Chapellier, B.; Deloche, B.; Oeser, R. Segmental order in uniaxially strained bimodal polymer networks: a deuterium-NMR study. *J. Phys. II* **1993**, *3*, 1619–1631.

- (25) Ries, M. E.; Brereton, M. G.; Klein, P. G.; Ward, I. M.; Ekanayake, P.; Menge, H.; Schneider, H. Contributions to the total orientation of deformed elastomers arising from the network structure and chain interactions as measured by NMR. *Macromolecules* **1999**, *32*, 4961–4968.
- (26) Hedden, R. C.; McCaskey, E.; Cohen, C.; Duncan, T. M. Effects of molecular structure on segment orientation in siloxane elastomers. 1. NMR measurements from compressed samples. *Macromolecules* **2001**, *34*, 3285–3293.
- (27) Callaghan, P. T.; Samulski, E. T. Biaxial deformation of a polymer network measured via deuteron quadrupolar interactions. *Macromolecules* **2003**, *36*, 724–735.
- (28) Rault, J.; Marchal, J.; Judeinstein, P.; Albouy, P. A. Stress-induced crystallization and reinforcement in filled natural rubbers: 2H NMR study. *Macromolecules* **2006**, *39*, 8356–8368.
- (29) Saalwächter, K.; Sommer, J.-U. NMR reveals non-distributed and uniform character of network chain dynamics. *Macromol. Rapid Commun.* **2007**, *28*, 1455–1465.
- (30) Saalwächter, K.; Herrero, B.; López-Manchado, M. A. Chain order and cross-link density of elastomers as investigated by proton multiple-quantum NMR. *Macromolecules* **2005**, *38*, 9650–9660.
- (31) Chassé, W.; Valentín, J. L.; Genesky, G. D.; Cohen, C.; Saalwächter, K. Precise dipolar coupling constant distribution analysis in proton multiple-quantum NMR of elastomers. *J. Chem. Phys.* **2011**, *134*, 044907.
- (32) Sommer, J.-U.; Chassé, W.; Valentín, J. L.; Saalwächter, K. Effect of excluded volume on segmental orientation correlations in polymer chains. *Phys. Rev. E* **2008**, *78*, 051803.
- (33) Rubinstein, M.; Colby, R. H. *Polymer Physics*, 1st ed.; Oxford University Press: Oxford, UK, 2003.
- (34) Valentín, J. L.; Posadas, P.; Fernández-Torres, A.; Malmierca, M. A.; González, L.; Chasse, W.; Saalwächter, K. Inhomogeneities and chain dynamics in diene rubbers vulcanized with different cure systems. *Macromolecules* **2010**, *43*, 4210–4222.
- (35) Saalwächter, K.; Kleinschmidt, F.; Sommer, J.-U. Swelling heterogeneities in end-linked model networks: A combined proton multiple-quantum NMR and computer simulation study. *Macromolecules* **2004**, *37*, 8556–8568.
- (36) Vieyres, A.; Pérez-Aparicio, R.; Albouy, P.-A.; Sanseau, O.; Saalwächter, K.; Long, D. R.; Sotta, P. Sulfur-cured natural rubber elastomer networks: Correlating cross-link density, chain orientation, and mechanical response by combined techniques. *Macromolecules* **2013**, *46*, 889–899.
- (37) Valentín, J. L.; Carretero-González, J.; Mora-Barrantes, I.; Chassé, W.; Saalwächter, K. Uncertainties in the determination of cross-link density by equilibrium swelling experiments in natural rubber. *Macromolecules* **2008**, *41*, 4717–4729.
- (38) Valentín, J. L.; Mora-Barrantes, I.; Carretero-González, J.; Lopez-Manchado, M. A.; Sotta, P.; Long, D. R.; Saalwächter, K. Novel experimental approach to evaluate filler-elastomer interactions. *Macromolecules* **2009**, *43*, 334–346.
- (39) Fetters, L. J.; Lohse, D. J.; Colby, R. H. Chain dimensions and entanglement spacings. In Mark, J. E., Ed.; *Physical Properties of Polymers Handbook*; Springer: New York, 2007; Chapter 25, pp 447–454.
- (40) Huneau, B. Strain-induced crystallization of natural rubber: A review of X-ray diffraction investigations. *Rubber Chem. Technol.* **2011**, *84*, 28.
- (41) Albouy, P.-A.; Guillier, G.; Petermann, D.; Vieyres, A.; Sanseau, O.; Sotta, P. A stroboscopic X-ray apparatus for the study of the kinetics of strain-induced crystallization in natural rubber. *Polymer* **2012**, *53*, 3313–3324.
- (42) Trabelsi, S.; Albouy, P. A.; Rault, J. Crystallization and melting processes in vulcanized stretched natural rubber. *Macromolecules* **2003**, *36*, 7624–7639.
- (43) Tosaka, M.; Senoo, K.; Sato, K.; Noda, M.; Ohta, N. Detection of fast and slow crystallization processes in instantaneously-strained samples of *cis*-1,4-polyisoprene. *Polymer* **2012**, *53*, 864–872.
- (44) Brüning, K.; Schneider, K.; Roth, S. V.; Heinrich, G. Kinetics of Strain-induced crystallization in natural rubber studied by WAXD: Dynamic and impact tensile experiments. *Macromolecules* **2012**, *45*, 7914–7919.
- (45) Dupres, S.; Long, D. R.; Albouy, P.-A.; Sotta, P. Local deformation in carbon black-filled polyisoprene rubbers studied by NMR and X-ray diffraction. *Macromolecules* **2009**, *42*, 2634–2644.
- (46) Mauri, M.; Thomann, Y.; Schneider, H.; Saalwächter, K. Spin-diffusion NMR at low field for the study of multiphase solids. *Solid State Nucl. Magn. Reson.* **2008**, *34*, 125–141.
- (47) Lequeux, F.; Long, D.; Sotta, P.; Saalwächter, K. Constrained dynamics in interphases of model filled elastomers: Role of interface chemistry on crosslinking, local stress distribution and mechanics. *Angew. Chem., Int. Ed.* **2011**, *50*, A63–A70.
- (48) Papon, A.; Saalwächter, K.; Schäler, K.; Guy, L.; Lequeux, F.; Montes, H. Low-Field NMR investigations of nanocomposites: Polymer dynamics and network effects. *Macromolecules* **2011**, *44*, 913–922.
- (49) Sotta, P.; Deloche, B. Uniaxiality induced in a strained poly(dimethylsiloxane) network. *Macromolecules* **1990**, *23*, 1999–2007.
- (50) Brereton, M. G. NMR study of the molecular anisotropy induced in a strained rubber network. *Macromolecules* **1993**, *26*, 1152–1157.
- (51) Jarry, J.-P.; Monnerie, L. Effects of a nematic-like interaction in rubber elasticity theory. *Macromolecules* **1979**, *12*, 316–320.
- (52) Wall, F. T.; Flory, P. J. Statistical thermodynamics of rubber elasticity. *J. Chem. Phys.* **1951**, *19*, 1435–1439.
- (53) Kuhn, W.; Grün, F. Beziehungen zwischen elastischen Konstanten und Dehnungsdoppelbrechung hochelastischer Stoffe. *Colloid Polym. Sci.* **1942**, *101*, 248–271.
- (54) Alexandre, J.; Marvão, M. R.; Feio, G. 2H NMR study of deformed natural rubber networks. *Mater. Sci. Forum* **2008**, *687*, 587–588.
- (55) Batra, A.; Hedden, R. C.; Schofield, P.; Barnes, A.; Cohen, C.; Duncan, T. M. Conformational behavior of guest chains in uniaxially stretched poly(diethylsiloxane) elastomers: 2H NMR and SANS. *Macromolecules* **2003**, *36*, 9458–9466.
- (56) Valic, S.; Sotta, P.; Deloche, B. 2H NMR study of a deformed poly(dimethylsiloxane) rubber network below and above the crystallization temperature. *Polymer* **1999**, *40*, 989–994.
- (57) Samulski, E. T. Investigations of polymer chains in oriented fluid phases with deuterium nuclear magnetic resonance. *Polymer* **1985**, *26*, 177–189.
- (58) Deloche, B.; Dubault, A.; Herz, J.; Lapp, A. Orientation of Free polymer chains dissolved in a strained elastomer: A deuterium magnetic-resonance. *Europhys. Lett.* **1986**, *1*, 629.
- (59) McLoughlin, K.; Waldbieser, J. K.; Cohen, C.; Duncan, T. M. End-linked poly(dimethylsiloxane) elastomers: 2H-nuclear magnetic resonance investigations of compression-induced segment anisotropy. *Macromolecules* **1997**, *30*, 1044–1052.
- (60) Cohen Addad, J. P.; Soyez, E. State of gelation of randomly crosslinked polybutadiene chains. Nuclear magnetic resonance, swelling, and elongation. *Macromolecules* **1992**, *25*, 6855–6865.
- (61) Genesky, G. D.; Duncan, T. M.; Cohen, C. Effect of precursor molar mass on the 2H NMR line shapes of end-linked PDMS elastomers. *Macromolecules* **2009**, *42*, 8882–8888.
- (62) Long, D.; Sotta, P. Stress relaxation of large amplitudes and long timescales in soft thermoplastic and filled elastomers. *Rheol. Acta* **2007**, *46*, 1029–1044.
- (63) Mujtaba, A.; Keller, M.; Ilisch, S.; Radusch, H.-J.; Thurn-Albrecht, T.; Saalwächter, K.; Beiner, M. Mechanical properties and cross-link density of styrene butadiene model composites containing fillers with bimodal particle size distribution. *Macromolecules* **2012**, *45*, 6504–6515.
- (64) Lang, M.; Sommer, J.-U. Analysis of entanglement length and segmental order parameter in polymer networks. *Phys. Rev. Lett.* **2010**, *104*, 177801.

- (65) Deloche, B.; Samulski, E. T. Rubber elasticity: a phenomenological approach including orientational correlations. *Macromolecules* **1988**, *21*, 3107–3111.
- (66) Oyerokun, F. T.; Schweizer, K. S. Microscopic theory of orientational order, structure and thermodynamics in strained polymer liquids and networks. *J. Chem. Phys.* **2004**, *120*, 475–485.
- (67) Chassé, W.; Schlogl, S.; Riess, G.; Saalwächter, K. Inhomogeneities and local chain stretching in partially swollen networks. *Soft Matter* **2013**, DOI: 10.1039/C3SM5019SG.
- (68) Baeza, G. P.; Genix, A. C.; Degrandcourt, C.; Petitjean, L.; Gummel, J.; Couty, M.; Oberdisse, J. Multiscale filler structure in simplified industrial nanocomposite silica/SBR systems studied by SAXS and TEM. *Macromolecules* **2013**, *46*, 317–329.